

# Suspensions of Semiconducting Nanoparticles in Nafion for Transient Spectroscopy and Terahertz Photoconductivity Measurements

Jacob A. Spies, Miryl J. Hilibrand, Jens Neu, Sarah Ostresh, John R. Swierk, and Charles A. Schmuttenmaer\*



Cite This: <https://dx.doi.org/10.1021/acs.analchem.9b05723>



Read Online

ACCESS |



Metrics & More

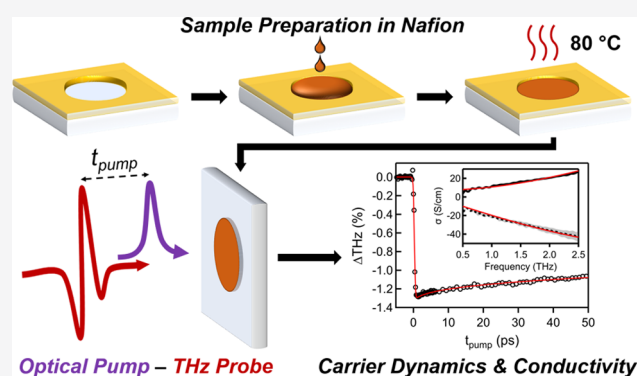


Article Recommendations



Supporting Information

**ABSTRACT:** The characterization of emerging materials is crucial for the experimentally driven design of next-generation technologies. We describe a cost- and time-effective method for suspending nanoparticles and other photoactive materials in Nafion for transient spectroscopy and time-resolved terahertz (THz) photoconductivity measurements. Nafion is an ideal suspension matrix because it has high transparency throughout the UV/vis/near-IR and THz regions of the spectrum. Suspensions of nanoparticles in Nafion require only small amounts of sample (<5 mg) and can be prepared and deposited in ~1 h. The suspension is well-suited for transient THz measurements, which can be used to determine the photoconductivity spectrum of the embedded nanoparticles. In this work, we used silicon nanoparticles as a model material to demonstrate the efficacy of Nafion suspensions for transient THz spectroscopy. This methodology can be used for rapid and cost-effective measurements of emerging materials such as solar materials, electrocatalysts, and nanomaterials.



Spectroscopic measurements are useful for characterizing materials and studying both their steady-state and dynamic properties. In particular, transient spectroscopic measurements based on pulsed lasers are a powerful tool for characterizing materials and provide insight into the dynamics of photo-induced processes on time scales ranging from attoseconds to milliseconds.<sup>1–5</sup> Reliable sample preparation for spectroscopy is the cornerstone of reproducible measurements and one of the first considerations addressed in an experiment. For solutions, the method of sample preparation is often clear, using a cuvette, flow cell,<sup>6</sup> or liquid jet.<sup>7</sup> However, solid-state samples, such as nanomaterials, are often much more challenging to prepare in a replicable fashion.

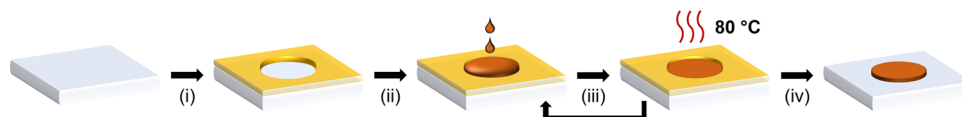
Whereas there are many methods to produce nanoparticle suspensions for transient spectroscopy, most are either too technically challenging to achieve reproducible samples, require a large amount of sample material, or are not sufficiently transparent to allow for photoexcitation.<sup>8–11</sup> Taking a cue from electrocatalysis, we report a method for preparing nanoparticle suspensions in a Nafion ink similar to that described in 2012 by Reier et al.<sup>12</sup> and others.<sup>13</sup> Nafion films have been utilized to study ionic complexes spectroscopically in the IR and near-IR, owing to their ion-exchange properties.<sup>14,15</sup> However, they have not been used to spectroscopically study suspended solid-state materials.

Nafion is frequently used in electrocatalysis and as a proton-exchange layer.<sup>12,16</sup> Therefore, processing techniques are well-established, and the material is commercially available with sufficient purity. Additionally, Nafion is transparent throughout the UV–visible region of the electromagnetic spectrum, making it ideally suited for optical spectroscopy. Nafion is also transparent in the THz regime (0.1–3 THz or ~3–100 cm<sup>-1</sup>), making it an ideal matrix for preparing samples for time-resolved terahertz (THz) spectroscopy (TRTS).<sup>17</sup> Finally, Nafion has a unique advantage in that it allows for the suspension of nanoparticles without making mesoporous nanoparticle films, which can be challenging to prepare, as they often require large amounts of material, require a relatively high temperature to anneal the film, and can be prone to “flaking off” the substrate.<sup>8</sup> Compared with other sample preparation methods involving a suspension in a polymer matrix, such as cyclic olefin copolymers<sup>11</sup> and Teflon,<sup>9,18</sup> using

Received: December 18, 2019

Accepted: February 24, 2020

Published: February 24, 2020

Scheme 1. Preparation of a Nanoparticle Suspension in Nafion Film for Spectroscopic Measurements<sup>a</sup>

<sup>a</sup>(i) Apply mask (Kapton tape), (ii) deposit Nafion ink, (iii) dry at 80 °C, (iv) remove mask. Step (iii) can be repeated to deposit thicker films.

Nafion as a matrix provides a fast ( $\sim 1$  h) and versatile preparation with no specialty equipment for the transient spectroscopy of nanoparticles in the solid state.

This work presents a procedure to prepare samples suspended in Nafion for transient spectroscopy, in particular, TRTS. TRTS, which is described in the [Supporting Information](#), is an ultrafast pump–probe technique that is sensitive to the transient photoconductivity (i.e., presence of photogenerated mobile carriers) of a semiconducting sample.<sup>19</sup> This work also delineates procedures for analyzing carrier dynamics and time-resolved photoconductivity in semiconducting, nanoparticulate samples without assuming any conductivity model whatsoever.<sup>20</sup> This method is broadly applicable to any studies requiring a robust solid-state sample preparation for spectroscopic measurements in the UV–visible or THz regions of the electromagnetic spectrum. Although not evaluated in this work, Nafion is also transparent through parts of the near- and mid-IR, making experiments in those regions also possible.<sup>14,15</sup> This method is useful for studying emerging materials (solar materials, electrocatalysts, nanomaterials, etc.) because it does not require a large amount of sample and can potentially be used to mimic operating conditions such as the inclusion of an electrolyte.

## EXPERIMENTAL SECTION

**Optimized Sample Preparation.** Nafion inks were prepared by mixing 3.00 mL of isopropyl alcohol (Sigma-Aldrich), 11.88 mL of 18.2 M $\Omega$ -cm water, 120  $\mu$ L of 5 wt % Nafion solution (Sigma-Aldrich), and an approximately 3:1 ratio by volume of nanoparticles to Nafion, in this case ( $2.53 \pm 0.03$ ):1, corresponding to  $15.7 \pm 0.1$  mg of polycrystalline Si nanoparticles (US Research Nanomaterials,  $\sim 30$  nm diameter) in a centrifuge tube. Then, the inks were sonicated using a horn sonifier (Branson Sonifier 450) for 10 min. It should be noted that this procedure can easily be scaled up or down depending on the scarcity of sample materials.

Quartz slides for sample deposition were cleaned with Alconox detergent, followed by rinsing with water, then isopropanol, dried with a stream of N<sub>2</sub>, and subsequently layered with a Kapton tape mask (five layers,  $\sim 0.35$  mm). A 1 cm<sup>2</sup> circle was cut from the tape with a razor blade and removed. The slides were placed onto a hot plate at 80 °C. 115  $\mu$ L of Nafion ink was then drop-casted in the circular well and dried at 80 °C. [Scheme 1](#) illustrates the deposition process.

Film thicknesses can be increased by subsequent drop-casting and drying until a desired thickness is reached. We found that the first layer deposited was the most crucial for uniform films. If the first layer is over dried, then the film tends to aggregate around the edges of the well, and subsequent layers deposit heterogeneously. For multilayer films, subsequent layers should be deposited immediately upon the previous layer visibly drying (usually 5–7 min). Once the final layer was deposited, a final drying time of 10–20 min was used. For TRTS measurements performed in this work, three-

layer samples were prepared. Details regarding the optimization process can be found in the [Supporting Information](#).

**Sample Characterization.** UV–visible transmittance spectra were collected using a Shimadzu UV-2600 spectrometer. Film thicknesses were measured using a Bruker Dektak mechanical profilometer. Optical metrology was performed with a Zygo Nexview 3D optical profiler. THz transmission spectra were collected with a home-built THz time-domain spectrometer (THz-TDS), as previously described.<sup>18,21,22</sup> Scanning electron microscopy images were collected using a Hitachi SU8230 cold field-emission scanning electron microscope. Powder X-ray diffraction (PXRD) measurements were performed using a Rigaku SmartLab X-ray diffractometer.

**Time-Resolved Terahertz Spectroscopy.** TRTS measurements were made as previously described.<sup>10,19,23</sup> A more detailed description of the spectrometer and experimental methodology can be found in the [Supporting Information](#). Samples were photoexcited using 400 nm light with a pump energy of 200  $\mu$ J/pulse and a spot size of  $8.56 \pm 0.10$  mm diameter, corresponding to a fluence of  $\sim 640 \mu$ J cm<sup>-2</sup> and a photon flux of  $1.3 \times 10^{15}$  cm<sup>-2</sup>. This visible wavelength was chosen due to its relevance in solar applications. Photoconductivity spectra of the Si nanoparticles were calculated numerically using Bruggeman effective medium theory (EMT) to account for the Si nanoparticles embedded in Nafion.<sup>20,22</sup>

## RESULTS AND DISCUSSION

**Nafion Film Characterization.** We used a variety of techniques for the metrology of the Si:Nafion films, as previously detailed. [Figure 1](#) presents a summary of the characterization results. [Figure 1a](#) shows a typical optical profilometry measurement of a three-layer film, and it is seen that the thickness in the center of the film is 2 to 4  $\mu$ m. There are a few minor heterogeneities along the film edges, which is consistent with the wetting issues previously discussed. However, the THz measurement spot size, as illustrated by the green circle, is  $\sim 1$  mm in diameter (see [Figure S1](#)) and probes a homogeneous region of the film. In addition, THz-TDS line scans such as that shown in [Figure 1b](#), which monitor the THz peak amplitude as a function of sample position, show little heterogeneity. [Figure 1c](#) shows an SEM image of the nanoscale surface morphology. We also examined a series of films as a function of the number of deposition steps via mechanical profilometry ([Figure 1d](#)).

The optical transmission spectrum of blank Nafion films is  $>90\%$  from 300 to 800 nm (see [Figure S3a](#)) for a sample with six times the amount of Nafion as those measured in this work. In the THz range, blank Nafion films exhibit unity transmission within our experimental uncertainty. (See [Figure S3b](#).)

Polycrystalline silicon nanoparticles were characterized by PXRD to determine their crystallinity and crystallite grain size using the Scherrer equation.<sup>24</sup> (See [Figure S4](#) and [Table S2](#).) We determined that the lower limit for the crystallite size was  $30 \pm 2$  nm, which is approximately the particle size specified by the manufacturer, implying near-single-crystallinity.

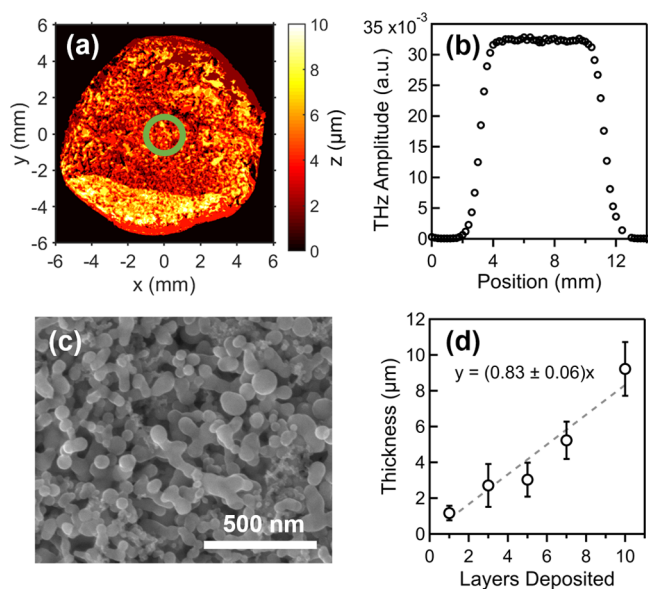


**Figure 1.** Characterization of Si:Nafion film morphology. (a) Representative three-layer film profile obtained using an optical profilometer. The green circle represents the THz probe spot size. (b) THz-TDS line scan across the center of the sample illustrates the homogeneity of a three-layer film sample to THz radiation. The copper sample holder, which has a diameter of 8.9 mm, blocks the transmission at the edges of the plot. (c) SEM image of a three-layer Si:Nafion film surface. (d) Si:Nafion film thickness measured using mechanical profilometry as a function of number of layers deposited with linear fit.

**Carrier Dynamics.** Optical pump-THz probe (OPTP) measurements, which is a subset of TRTS wherein the maximum amplitude of the THz pulse is measured as a function of pump-probe delay time (see Figure S1a), were carried out to assay the efficacy of this technique to study carrier dynamics in nanoparticulate samples suspended in Nafion. Figure 2 shows a representative OPTP measurement of a Si:Nafion sample as well as a pure Nafion film, which is shown in the inset.

The data (black circles) were fit with a stretched exponential function (eq 1), where  $\Delta\text{THz}$  is the percent change in THz

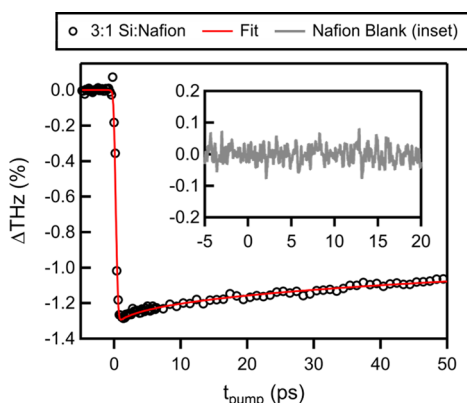


**Figure 2.** Representative optical pump-THz probe measurement of Si:Nafion fit with a stretched exponential function (black circles and red line, respectively). The inset (gray line) is that for a blank Nafion sample, illustrating that it does not have a photoinduced THz response.

transmission,  $A$  is the amplitude of the exponential,  $t_{\text{pump}}$  is the pump pulse time delay,  $\tau$  is the lifetime,  $\beta$  is the stretch exponent (which was fixed at 0.4 for all fits),  $\otimes$  represents a convolution, and  $G_{\text{IRF}}$  is a Gaussian instrument response function with a 0.6 ps full width at half-maximum.<sup>25</sup>

$$\Delta\text{THz} = \left[ A \exp\left(\left(\frac{-t_{\text{pump}}}{\tau}\right)^\beta\right) \right] \otimes G_{\text{IRF}} \quad (1)$$

OPTP measurements of a pure Nafion film (inset, gray line) do not show any photoinduced signal, confirming that the measured signal for Si:Nafion results from photoinduced carriers in the Si nanoparticles. Bulk, single-crystal Si exhibits a  $200 \pm 30 \mu\text{s}$  carrier lifetime. (See the Supporting Information for details.) The measurements shown in Figure 2 depict a relatively fast trapping lifetime of  $6 \pm 2 \text{ ns}$  (calculated stretched exponential lifetime expectation value;<sup>25</sup> see Table S3). A comparison with a single-crystal Si wafer, illustrating differences in carrier lifetime, is shown in Figure S5. Although the absolute quantification of the carrier lifetime in Si nanoparticles suspended in Nafion is outside the scope of this methodological report, the dynamics show good agreement with previously reported results for nanocrystalline silicon.<sup>26</sup> The results in Figure 2 and their agreement with literature values demonstrate that suspending photoactive materials in Nafion is a viable method for studying carrier dynamics and other transient processes.

**Frequency-Dependent Photoconductivity.** In addition to studying carrier dynamics via OPTP, TRTS was utilized to measure the photoconductivity of Si:Nafion at a pump-probe delay ( $t_{\text{pump}}$ ) of 10 ps. The film thicknesses used in the numerical photoconductivity calculation were obtained from averaging the center 2 mm section of film profiles obtained by mechanical profilometry (see the inset values in Figure S8) using Bruker Vision64 data collection and analysis software.

Bruggeman EMT was utilized for a number of steps to extract the frequency-dependent photoconductivity spectrum. In brief, EMT describes effective optical constants for a mixture of materials by taking into account the optical constants for an inclusion (silicon) and a host material (Nafion) and their volume fractions. The functional form of Bruggeman EMT is shown in eq 2, where  $f$  is the volume fraction of the inclusion (determined to be  $0.717 \pm 0.003$  using the relative masses and densities of Si and Nafion for this experiment),  $\epsilon_{\text{inc}}$  is the complex permittivity of the inclusion material,  $\epsilon_{\text{host}}$  is the complex permittivity of the host material, and  $\epsilon_{\text{eff}}$  is the complex effective permittivity. It should be noted that the permittivity ( $\epsilon$ ) is related to the complex refractive index ( $n$ ) of a nonmagnetic material by  $\epsilon = n^2$ .

$$f \frac{\epsilon_{\text{inc}} - \epsilon_{\text{eff}}}{\epsilon_{\text{inc}} + 2\epsilon_{\text{eff}}} + (1 - f) \frac{\epsilon_{\text{host}} - \epsilon_{\text{eff}}}{\epsilon_{\text{host}} + 2\epsilon_{\text{eff}}} = 0 \quad (2)$$

To extract the photoconductivity spectrum shown in Figure 3, a reference measurement of the nonphotoexcited sample and a difference measurement of the photoexcited sample (i.e., the difference between pump-on and pump-off) were measured. The photoexcited response can then be extracted by an addition of the two measurements. After Fourier transformation, the experimental complex transmission function ( $T_{\text{exp}}$ ), is obtained as shown in eq 3, where  $E_{\text{on}}$  and  $E_{\text{off}}$  are the photoexcited and nonphotoexcited transmission amplitudes, respectively.

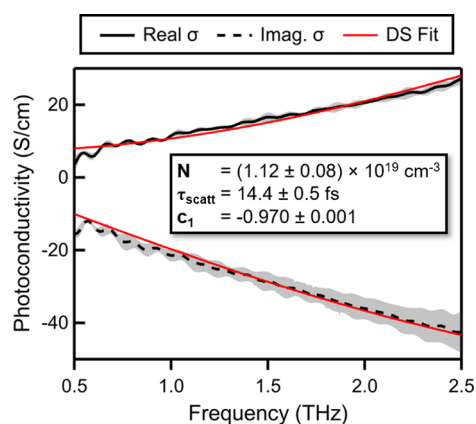


**Figure 3.** Frequency-dependent photoconductivity spectrum of Si:Nafion at  $t_{\text{pump}} = 10$  ps (black solid and dashed lines) determined using EMT without a conductivity model. The photoconductivity spectrum was then fit with the Drude–Smith (DS) model with the fit coefficients shown in the inset, where  $N$  is the carrier density,  $\tau_{\text{scatt}}$  is the scattering time, and  $c_1$  is the “persistence of velocity” parameter. Errors reported in fit parameters are confidence intervals of the fit. Shading represents one standard deviation of the four independent samples averaged.

$$T_{\text{exp}}(\omega) = \frac{E_{\text{on}}(\omega)}{E_{\text{off}}(\omega)} \quad (3)$$

It is possible to calculate the transmission function based on the geometry of the sample using a propagation operator and the Fresnel coefficients describing transmission and reflection.<sup>20,22</sup> Because the sample is thin with respect to the THz time trace (i.e., all internal reflections are collected), a Fabry–Pérot etalon term ( $FP_{ijk}$ ) must also be included. Details regarding the sample geometry, Fresnel coefficient, Fabry–Pérot etalon term, and formulation of the transmission function are included in the [Supporting Information](#). It should be noted that because the sample geometry is not symmetric, the transmission direction and photoexcitation direction must be considered when constructing the transfer function. In addition, the pump-beam penetration length was determined to be  $0.1429 \pm 0.0005 \mu\text{m}$  using literature refractive index values for Si and Nafion and EMT.<sup>27–29</sup> In the case where the penetration length is less than the film thickness, an additional interface is present in the photoexcited sample. (See [Figure S2](#).)

The theoretical transmission function,  $T_{\text{theo}}$ , used for these films is shown in [eq 4](#). In this equation,  $n_p$  is the effective photoexcited refractive index,  $n_n$  is the effective non-photoexcited refractive index calculated from literature values and EMT,<sup>17,29,30</sup>  $n_a$  is the refractive index of air,  $k_0$  is the THz-wavevector in vacuum,  $d_p$  is the penetration length, and  $FP$  are Fabry–Pérot terms, all of which are detailed in the [Supporting Information](#).

$$T_{\text{theo}} = \left( \frac{2n_p}{n_p + n_n} \right) \left( \frac{n_n + n_a}{n_p + n_a} \right) \exp[ik_0 d_p (n_n - n_p)] \left( \frac{FP_{apn} FP_{pn'q}}{FP_{anq}} \right) \quad (4)$$

The effective photoexcited refractive index,  $n_p$ , was extracted by numerically solving  $T_{\text{exp}} = T_{\text{theo}}$  for  $n_p$  using the Optimization Toolbox in MATLAB.

Once  $n_p$  was determined, the refractive index of the photoexcited Si inclusions ( $n_{\text{on}}$ ) was extracted using EMT

and the refractive index of Nafion as obtained from literature values.<sup>17</sup> Because Nafion does not have a photoinduced response, the photoexcited and nonphotoexcited refractive indices are the same. The photoconductivity spectrum was extracted from  $n_{\text{on}}$  using [eq 5](#), where  $n_{\text{off}}$  is the non-photoexcited refractive index of silicon,<sup>30</sup>  $\sigma$  is the photoconductivity,  $\omega$  is the angular frequency, and  $\epsilon_0$  is the vacuum permittivity.

$$n_{\text{on}}^2 = n_{\text{off}}^2 + \frac{i\sigma(\omega, t_{\text{pump}})}{\epsilon_0\omega} \quad (5)$$

The extracted photoconductivity spectrum,  $\sigma$ , was then fit with the Drude–Smith (DS) model, as shown in [eq 6](#).<sup>31</sup>  $N$  is the carrier density,  $e$  is the fundamental unit of charge,  $\tau_{\text{scatt}}$  is the scattering time,  $m^*$  is the effective carrier mass ( $0.19m_e$  for silicon, where  $m_e$  is the mass of an electron),<sup>32</sup> and  $c_1$  is the “persistence of velocity” parameter.<sup>25,33</sup>

$$\sigma(\omega, t_{\text{pump}}) = \frac{Ne^2\tau_{\text{scatt}}/m^*}{1 - i\omega\tau_{\text{scatt}}} \left( 1 + \frac{c_1}{1 - i\omega\tau_{\text{scatt}}} \right) \quad (6)$$

The results of the numerical calculation for four independent samples were averaged and fit with [eq 6](#) and are plotted in [Figure 3](#). The independent measurements and fits are shown in the [Supporting Information](#). The strong advantage of THz spectroscopy can be seen in the fact that the real and imaginary parts of the conductivity are simultaneously retrieved. In contrast, DC measurements cannot provide temporal resolution, and optical techniques fail to provide broadband real and imaginary contributions. The experimentally determined values from the Drude–Smith fit are in good agreement with the literature values of nanocrystalline silicon.<sup>34</sup>

In addition to the numerical photoconductivity determination previously detailed, we also extracted the conductivity with the often-utilized thin-film approximation, which is based on a thin superconducting layer on a substrate.<sup>35</sup> Whereas this approximation is computationally simple, the assumption of the sample being a thin superconducting layer upon photoexcitation is not necessarily reasonable.<sup>20</sup> In this work, however, the penetration length used is much smaller than the film thickness, and thus the thin-film approximation provides reasonably close results. (See the [Supporting Information](#) for comparison.) However, caution is advised when using this approximation in other cases, as its reliability varies dramatically with the thickness of the sample and the optical penetration depth. We recommend avoiding the thin-film approximation and using the more rigorous numerical treatment previously described for extracting the photoconductivity spectrum, especially as the sample geometry becomes more complex.<sup>20</sup>

## CONCLUSIONS

This work describes a reliable sample fabrication technique for transient spectroscopy and THz photoconductivity measurements based on embedding nanomaterials in transparent Nafion films. This method provides a cost-effective alternative for the sample preparation of materials available in only small (i.e., milligram) quantities. We demonstrate that films of differing thicknesses can be fabricated using only small amounts of material (<5 mg) and that sample fabrication can be performed at moderate temperatures (80 °C) and can be completed in under 1 h.

We have demonstrated the efficacy of this technique using silicon nanoparticles. The resulting films were characterized using SEM, mechanical profilometry, optical profilometry, UV–vis spectroscopy, and time-resolved THz spectroscopy (OTPT and transient photoconductivity). The optical properties of the photoexcited Si nanoparticles embedded in the Nafion film were determined using Bruggeman EMT, and the material parameters retrieved were in good agreement with literature values. This technique can be straightforwardly applied to a range of materials. It also serves as an excellent method for preparing samples of strongly absorbing materials, which need to be diluted for proper spectroscopic measurements.

## ■ ASSOCIATED CONTENT

### SI Supporting Information

The Supporting Information is available free of charge at <https://pubs.acs.org/doi/10.1021/acs.analchem.9b05723>.

Additional experimental details and information on numerical data processing, additional materials characterization, supplemental time-resolved THz spectroscopy results and fit parameters, and comparison of numerical photoconductivity processing and thin-film photoconductivity processing (PDF)

## ■ AUTHOR INFORMATION

### Corresponding Author

Charles A. Schmuttenmaer – Department of Chemistry and Energy Sciences Institute, Yale University, New Haven, Connecticut 06520, United States; [orcid.org/0000-0001-9992-8578](https://orcid.org/0000-0001-9992-8578); Email: [charles.schmuttenmaer@yale.edu](mailto:charles.schmuttenmaer@yale.edu)

### Authors

Jacob A. Spies – Department of Chemistry and Energy Sciences Institute, Yale University, New Haven, Connecticut 06520, United States; [orcid.org/0000-0002-0148-4823](https://orcid.org/0000-0002-0148-4823)

Miryl J. Hilibrand – Department of Chemistry and Energy Sciences Institute, Yale University, New Haven, Connecticut 06520, United States

Jens Neu – Department of Molecular Biophysics and Biochemistry and Microbial Sciences Institute, Yale University, New Haven, Connecticut 06520, United States; [orcid.org/0000-0002-1054-0444](https://orcid.org/0000-0002-1054-0444)

Sarah Ostresh – Department of Chemistry and Energy Sciences Institute, Yale University, New Haven, Connecticut 06520, United States

John R. Swierk – Department of Chemistry and Energy Sciences Institute, Yale University, New Haven, Connecticut 06520, United States; [orcid.org/0000-0001-5811-7285](https://orcid.org/0000-0001-5811-7285)

Complete contact information is available at:

<https://pubs.acs.org/10.1021/acs.analchem.9b05723>

### Notes

The authors declare no competing financial interest. The MATLAB script used for numerical data processing can be downloaded freely via our homepage at [thz.yale.edu](http://thz.yale.edu).

## ■ ACKNOWLEDGMENTS

This work was funded by the U.S. Department of Energy Office of Science, Office of Basic Energy Sciences (DOE DE-FG02-07ER15909) and by a generous donation from the TomKat Charitable Trust. J.A.S. acknowledges support from

the Onsager Graduate Research Fellowship in Chemistry. J.N. acknowledges support from the National Science Foundation (NSF CHE-1465085). SEM and XRD work were carried out with assistance from Dr. Min Li at the Yale West Campus Materials Characterization Core.

## ■ REFERENCES

- (1) Berera, R.; van Grondelle, R.; Kennis, J. T. M. *Photosynth. Res.* **2009**, *101*, 105–118.
- (2) Ramasesha, K.; Leone, S. R.; Neumark, D. M. *Annu. Rev. Phys. Chem.* **2016**, *67*, 41–63.
- (3) Schmuttenmaer, C. A. *Chem. Rev.* **2004**, *104*, 1759–1780.
- (4) Farr, E. P.; Quintana, J. C.; Reynoso, V.; Ruberry, J. D.; Shin, W. R.; Swartz, K. R. *J. Chem. Educ.* **2018**, *95*, 864–871.
- (5) Neu, J.; Rahm, M. *Opt. Express* **2015**, *23*, 12900–9.
- (6) Bredenbeck, J.; Hamm, P. *Rev. Sci. Instrum.* **2003**, *74*, 3188–3189.
- (7) Kondoh, M.; Tsubouchi, M. *Opt. Express* **2014**, *22*, 14135–14147.
- (8) Ito, S.; Chen, P.; Comte, P.; Nazeeruddin, M. K.; Liska, P.; Pechy, P.; Gratzel, M. *Prog. Photovoltaics* **2007**, *15*, 603–612.
- (9) Neu, J.; Nemes, C. T.; Regan, K. P.; Williams, M. R. C.; Schmuttenmaer, C. A. *Phys. Chem. Chem. Phys.* **2018**, *20*, 276–283.
- (10) Pattengale, B.; Neu, J.; Ostresh, S.; Hu, G.; Spies, J. A.; Okabe, R.; Brudvig, G. W.; Schmuttenmaer, C. A. *J. Am. Chem. Soc.* **2019**, *141*, 9793–9797.
- (11) Diaz-Albarran, L. M.; Lugo-Hernandez, E.; Ramirez-Garcia, E.; Enciso-Aguilar, M. A.; Valdez-Perez, D.; Cereceda-Company, P.; Granados, D.; Costa-Krämer, J. L. *Microelectron. Eng.* **2018**, *191*, 84–90.
- (12) Reier, T.; Oezaslan, M.; Strasser, P. *ACS Catal.* **2012**, *2*, 1765–1772.
- (13) Martin, C. R.; Rhoades, T. A.; Ferguson, J. A. *Anal. Chem.* **1982**, *54*, 1639–1641.
- (14) Krausz, E. *Chem. Phys. Lett.* **1985**, *120*, 113–117.
- (15) Krausz, E. R.; Mau, A. W. H. *Inorg. Chem.* **1986**, *25*, 1484–1488.
- (16) Kraytsberg, A.; Ein-Eli, Y. *Energy Fuels* **2014**, *28*, 7303–7330.
- (17) Yurchenko, S. O.; Zaytsev, K. I. *J. Appl. Phys.* **2014**, *116*, 113508.
- (18) Neu, J.; Stone, E. A.; Spies, J. A.; Storch, G.; Hatano, A. S.; Mercado, B. Q.; Miller, S. J.; Schmuttenmaer, C. A. *J. Phys. Chem. Lett.* **2019**, *10*, 2624–2628.
- (19) Beard, M. C.; Turner, G. M.; Schmuttenmaer, C. A. *Phys. Rev. B: Condens. Matter Mater. Phys.* **2000**, *62*, 15764–15777.
- (20) Neu, J.; Regan, K. P.; Swierk, J. R.; Schmuttenmaer, C. A. *Appl. Phys. Lett.* **2018**, *113*, 233901.
- (21) Williams, M. R. C.; Aschaffenburg, D. J.; Ofori-Okai, B. K.; Schmuttenmaer, C. A. *J. Phys. Chem. B* **2013**, *117*, 10444–10461.
- (22) Neu, J.; Schmuttenmaer, C. A. *J. Appl. Phys.* **2018**, *124*, 231101.
- (23) Jiang, J.; Spies, J. A.; Swierk, J. R.; Matula, A. J.; Regan, K. P.; Romano, N.; Brennan, B. J.; Crabtree, R. H.; Batista, V. S.; Schmuttenmaer, C. A.; Brudvig, G. W. *J. Phys. Chem. C* **2018**, *122*, 13529–13539.
- (24) Scherrer, P. *Nachr. Ges. Wiss. Goettingen, Math.-Phys. Kl.* **1918**, *2*, 98–100.
- (25) Regan, K. P.; Koenigsmann, C.; Sheehan, S. W.; Konezny, S. J.; Schmuttenmaer, C. A. *J. Phys. Chem. C* **2016**, *120*, 14926–14933.
- (26) Němec, H.; Zajac, V.; Kužel, P.; Malý, P.; Gutsch, S.; Hiller, D.; Zacharias, M. *Phys. Rev. B: Condens. Matter Mater. Phys.* **2015**, *91*, 195443.
- (27) Green, M. A.; Keevers, M. J. *Prog. Photovoltaics* **1995**, *3*, 189–192.
- (28) Peters, S. A. Water Sorption, Viscoelastic, and Optical Properties of Thin Nafion Films. Ph.D. Dissertation, The Pennsylvania State University, 2013.
- (29) Markel, V. A. *J. Opt. Soc. Am. A* **2016**, *33*, 1244–1256.

- (30) Grischkowsky, D.; Keiding, S. R.; van Exter, M.; Fattinger, C. J. *Opt. Soc. Am. B* **1990**, *7*, 2006–2015.
- (31) Smith, N. V. *Phys. Rev. B: Condens. Matter Mater. Phys.* **2001**, *64*, 155106.
- (32) Kittel, C. *Introduction to Solid State Physics*, 8th ed.; John Wiley & Sons: Hoboken, NJ, 2005.
- (33) Cocker, T. L.; Baillie, D.; Buruma, M.; Titova, L. V.; Sydora, R. D.; Marsiglio, F.; Hegmann, F. A. *Phys. Rev. B: Condens. Matter Mater. Phys.* **2017**, *96*, 205439.
- (34) Cooke, D. G.; MacDonald, A. N.; Hryciw, A.; Wang, J.; Li, Q.; Meldrum, A.; Hegmann, F. A. *Phys. Rev. B: Condens. Matter Mater. Phys.* **2006**, *73*, 193311.
- (35) Glover, R. E.; Tinkham, M. *Phys. Rev.* **1957**, *108*, 243–256.